Electronic Supplementary Material (ESI) for ChemComm.

Electronic Supporting Information (ESI)

Mn^{2+} and Ag^{+} luminescence-colour-changing sensing based on white-light-emitting lanthanide coordination polymer

Yu-xin Li, Shang-ju Li, Peng-fei Yan, Xin-yu Wang, Xu Yao, Guang-hui An and Guang-ming Li*

Content

1. Experimental section

1.1 Materials and instrumentation

1.2 Synthesis of the complexes **1** – **4**

2. Results and discussion

2.1 Crystallographic data, selected bonds lengths (Å) and bonds angles (º) for **1** – **3**

2.2 3D structure of the complexes

2.3 FT-IR, UV, TG-DSC and PXRD spectra for complexes **1** – **4**

2.4 Luminescent properties of **1** – **4**

2.5 Ag^{+} and Mn^{2+} sensing properties of **4**

1. Experimental section

1.1 Materials and Instrumentation

The commercially available chemicals were of analytical reagent grade and used without further purification. L-DBTA (99 %, Scheme S1) was purchased from Aladdin Co. (Shanghai, China). $LnCl_3 \cdot 6H_2O$ was prepared according to the literature by dissolving 99.99 % oxide in a slight excess of hydrochloric acid.[1] The solution was evaporated and the precipitate was recrystallized from water.

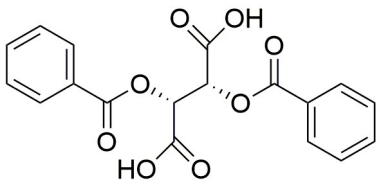

Scheme S1. The structure of the ligand L-DBTA

Elemental (C, H, N and O) analyses were performed with an Elementar Vario EL cube analyser. Fourier transform infrared (FT-IR) spectra were obtained on a Perkin-Elmer Spectrum One spectrophotometer by using KBr disks in the range of 4000 – 450 cm^{-1}. Ultraviolet (UV) spectra were recorded on a Perkin-Elmer Lambda 25 spectrometer. Thermal analyses were conducted on a Perkin-Elmer STA 6000 with a heating rate of 10 ºC · min^{-1} in a temperature range from 30 to 800 ºC under air atmosphere. Powder X-ray diffraction (PXRD) data were recorded on a Rigaku D/Max-3B X-ray diffractometer with Cu Kα as the radiation source (λ = 0.15406 nm) in the angular range of θ = 10 – 60 º. Crystal data of the complexes were collected using a Xcalibur, Eos, Gemini diffractometer with Mo Kα radiation (λ = 0.71073 Å). All data were collected at a temperature of 23 ± 2 ºC. The structures were solved by the direct methods and refined on F2 by full-matrix least-squares using the SHELXTL-97 program. The Ln (III) ions were easily located and then non-hydrogen atoms (C, N and O) were placed from the subsequent Fourier-difference maps. All non-hydrogen atoms were refined anistropically. A summary of data collection and refinements is given in Table S1 and S2. Excitation and emission spectra were measured with an Edinburgh FLS 920 fluorescence spectrophotometer. Luminescence lifetimes were recorded with a single photon counting spectrometer from Edinburgh Instruments (FLS920) with a microsecond pulse lamp and a picosecond laser as the excitation sources. The data were analysed by software supplied by Edinburgh Instrucments. The quantum yields for the complexes were determined at room temperature through an absolute method using an Edinburgh Instruments' integrating sphere coupled to a modular Edinburgh FLS 920 fluorescence spectrophotometer. The values reported are the

averge of three independent determinations for each sample. The absolute quantum yield was calculated using the following expression:

$$\Phi = \frac{\int L_{\text{emission}}}{\int E_{\text{reference}} - \int E_{sample}} \quad (1)$$

where L_{emission} is the emission spectrum of the sample, collected using the sphere, E_{sample} is the spectrum of the incident light used to excite the sample, collected using the sphere, and $E_{\text{reference}}$ is the spectrum of the light used for excitation with only the reference in the sphere. The method is accurate to within 10 %. The commission Internationale de I'Eclairage (CIE) color coordination was calculated on the basis of the international CIE standards.[2]

1.2 Synthesis of the complexes 1 – 4

A mixture of L-DBTA (0.358 g, 1 mmol) and triethylamine (Et_3N, 0.2 g, 2 mmol) in methanol (8 ml) was stirred for ten minutes at room temperature. Then the solution was slowly diffused into a 15 mm × 150 mm test tube, which was already added to a solution of $LnCl_3 \cdot 6H_2O$ (0.66 mmol) in H_2O (8 ml). Crystals suitable for X-ray determination were obtained in two days.

For the complexes **4**, the synthetic methods are the same as the aforementioned, except that the lanthanide salt solution is replaced by a mixed solution, according to the molar ratio in Sm:Eu:Tb = 1:1:3.

$\{Et_3NH[Sm(L\text{-}DBTA)_2(CH_3OH)_2(H_2O)_2]\cdot 2H_2O\}_n$ (**1**). Yield: 0.409 g (57.0 wt%). Anal. Calcd. for $C_{44}H_{56}NO_{22}Sm$ (wt %): C, 47.99; H, 5.13; N, 1.27; O, 32.3. Found (wt %): C, 48.01; H, 5.11; N, 1.31; O 32.3. IR (KBr pellet, cm^{-1}): 3369(s, $\nu_{O\text{-}H}$), 1720(s, $\nu_{C=O}$), 1602(s, $\nu_{C=O}$), 1433(m), 1272(s), 1123(s). UV–vis (MeOH, nm): 230, 274, 281.

$\{Et_3NH[Eu(L\text{-}DBTA)_2(CH_3OH)_2(H_2O)_2]\cdot 2H_2O\}_n$ (**2**). Yield: 0.398 g (54.7 wt%). Anal. Calcd. for $C_{44}H_{56}NO_{22}Eu$ (wt %): C, 47.92; H, 5.12; N, 1.27; O, 32.2. Found (wt %): C 47.79; H, 5.16; N, 1.22; O, 32.1. IR (KBr pellet, cm^{-1}): 3328(s, $\nu_{O\text{-}H}$), 1720(s, $\nu_{C=O}$), 1602(s, $\nu_{C=O}$), 1451(m), 1271(s), 1120(s). UV–vis (MeOH, nm): 231, 274, 281.

$\{Et_3NH[Tb(L\text{-}DBTA)_2(CH_3OH)_2(H_2O)_2]\cdot 2H_2O\}_n$ (**3**). Yield: 0.388 g (53.0 wt%). Anal. Calcd. for $C_{44}H_{56}NO_{22}Tb$ (wt %): C, 47.62; H, 5.09; N, 1.26; O, 32.0. Found (wt %): C, 47.70; H, 5.11; N, 1.20; O,

32.1. IR (KBr pellet, cm^{-1}): 3328(s, ν_{O-H}), 1721(s, $\nu_{C=O}$), 1603(s, $\nu_{C=O}$), 1451(m), 1272(s), 1119(s). UV–vis (MeOH, nm): 230, 274, 281.

$\{Et_3NH[(Sm_{0.2}Eu_{0.2}Tb_{0.6})(L\text{-}DBTA)_2(CH_3OH)_2(H_2O)_2]\cdot 2H_2O\}_n$ (**4**). Yield: 0.340 g (46.6 wt%). Anal. Calcd. for $C_{44}H_{56}NO_{22}Sm_{0.2}Eu_{0.2}Tb_{0.6}$ (wt %): C, 47.75; H, 5.10; N, 1.27; O, 31.80. Found (wt %): C, 47.70; H, 5.11; N, 1.27; O, 32.03. IR (KBr pellet, cm^{-1}): 3328(s, ν_{O-H}), 1721(s, $\nu_{C=O}$), 1603(s, $\nu_{C=O}$), 1451(m), 1272(s), 1119(s). UV–vis (MeOH, nm): 230, 274, 281.

2. Results and discussion

2.1 Crystallographic data, selected bonds lengths (Å) and bonds angles (°) for 1 – 3

Table S1. Crystallographic data for **1** – **3**

Parameters	**1** (Sm)	**2** (Eu)	**3** (Tb)
Empirical formula	$C_{44}H_{56}NO_{22}Sm$	$C_{44}H_{56}NO_{22}Eu$	$C_{44}H_{56}NO_{22}Tb$
Formula weight	1101.25	1102.86	1109.82
Temperature (K)	293(2) K	293(2) K	293(2) K
Wavelength (Å)	0.71073	0.71073	0.71073
Crystal system	Orthorhombic	Orthorhombic	Orthorhombic
Space group	$P2_12_12$	$P2_12_12$	$P2_12_12$
a(Å)	20.118(4)	20.072(4)	20.056(4)
b(Å)	16.652(3)	16.329(4)	16.412(3)
c(Å)	16.747(3)	16.631(4)	16.648(3)
Volume ($Å^3$)	5610.1(19)	5451(2)	5479.7(19)
Z	4	4	4
Calculated density Mg/m^3	1.304	1.344	1.345
Absorption coefficient(mm^{-1})	1.118	1.224	1.363
F(000)	2260	2264	2272
Reflections collected	50255	41969	51678
Max. and min. transmission	0.7667/ 0.7289	0.7990/0.7594	0.7914/0.7400
Data / restraints / parameters	12840 / 73 / 616	9533 / 64 / 617	12432 / 74 / 616
Goodness-of-fit on F^2	1.064	1.052	1.071
R1, wR2(I>2σ(I))	0.0585, 0.1770	0.0471, 0.1341	0.0679, 0.1853
R1, wR2(all data)	0.0854, 0.0854,	0.0577, 0.1424	0.0895, 0.2020
Δρ (e $Å^{-3}$)	1.453 and -1.166	1.253 and -1.158	1.585 and -2.553

Table S2. Selected bonds lengths (Å) and bonds angles (°) for **1** – **3**

Bonds	**1** (Sm)	**2** (Eu)	**3** (Tb)
Ln(1)–O(16)	2.397(5)	2.390(4)	2.346(5)
Ln(1)–O(8)	2.419(4)	2.407(4)	2.395(5)
Ln(1)–O(18)	2.460(5)	2.442(5)	2.398(6)
Ln(1)–O(17)	2.439(5)	2.424(4)	2.386(5)
Ln(2)–O(12)	2.371(4)	2.368(4)	2.344(5)
Ln(2)–O(4)	2.396(5)	2.379(4)	2.366(6)
Ln(2)–O(19)	2.481(5)	2.484(4)	2.445(6)
Ln(2)–O(20)	2.448(5)	2.430(5)	2.407(6)
O(16)–Ln(1)–O(16)	75.7(2)	76.91(19)	75.5(2)
O(8)–Ln(1)–O(8)	76.5(2)	77.0(2)	76.5(3)
O(4)–Ln(2)–O(4)	78.0(3	78.2(2)	77.0(3)
O(12)–Ln(2)–O(12)	79.5(2)	80.3(2)	78.9(3)

2.2 3D structure of the complexes

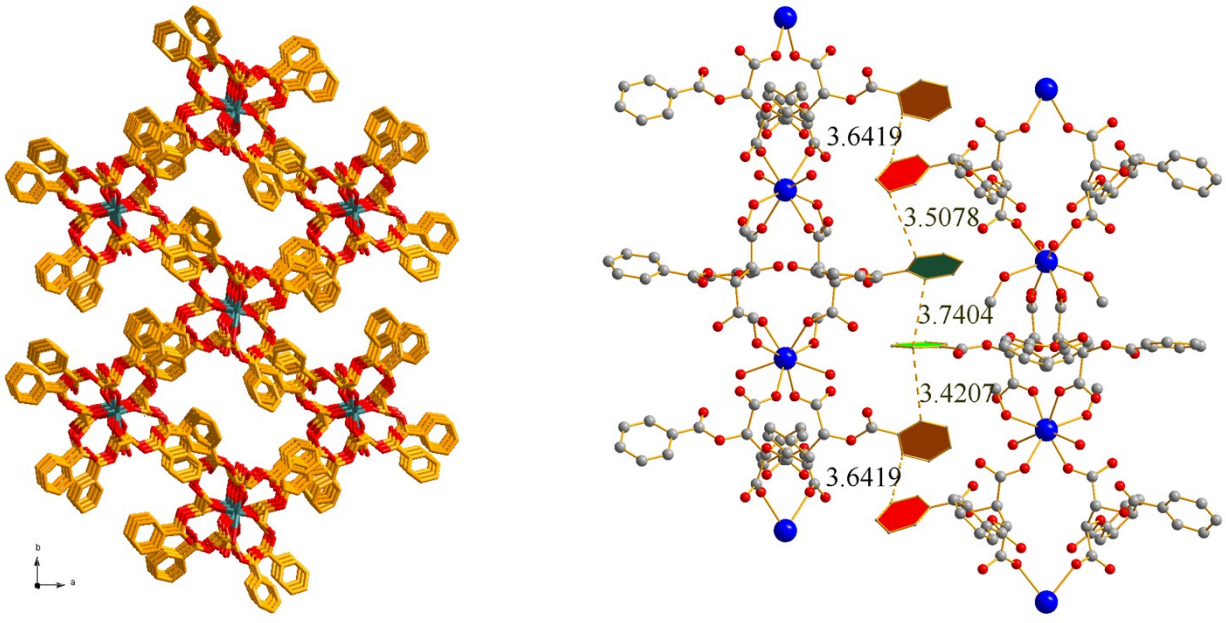

a b

Figure S1. a) 3D structure of complex **2** along the *c* axis. All H atoms are omitted for clarity; b) π-π stacking of the benzyl groups down the [110] direction

2.3 FT-IR, UV, TG-DSC and PXRD spectra for complexes 1 – 4

The FT-IR spectra of complexes **1** – **4** show similar patterns (Figure S2 and Table S3). In a typical spectrum of complex **2**, the broad band around 3328 cm^{-1} is attributed to the characteristic peak of O-H bonds from the solvent molecules in the complex. The asymmetric and symmetric stretching vibrations of carboxylate groups are observed at 1720, 1602, and 1451 cm^{-1}. The appearance of the characteristic band at 1602 cm^{-1} indicates the deprotonation of the carboxylate groups and coordination to the lanthanide ions. UV-vis absorption spectra of the L-DBTA and complexes **1** – **4** in methanol solution exhibit similar absorbance bands (Figure S3). The main absorption bands at 231 nm and 274 nm are attributed to the π-π* and n-π* transitions of the benzene ring, respectively. Thermal analyses support that there are crystalline solvents in complexes **1** – **4** (Figure S4). For example, complex **2** exhibits a gradual weight loss of 12.5 % in the temperature range of 30 – 120 ^{o}C, which corresponds to the loss of solvent molecules in complex **2** (calculated 12.3 %). Other calculations for crystalline solvents in complexes **1** – **4** are shown in Figure S4. PXRD analyses demonstrate that the structures of complexes **1** – **4** are isomorphic and their phase purity was verified by PXRD analyses (Fig. S5).

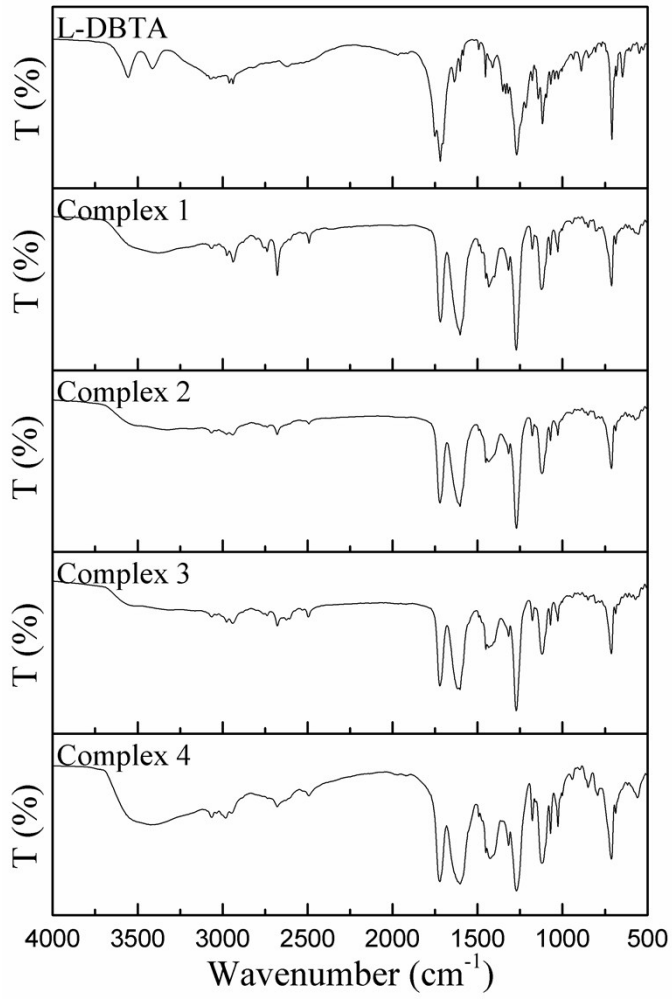

Figure S2. FT-IR spectra of ligand L-DBTA and complexes **1** – **4**

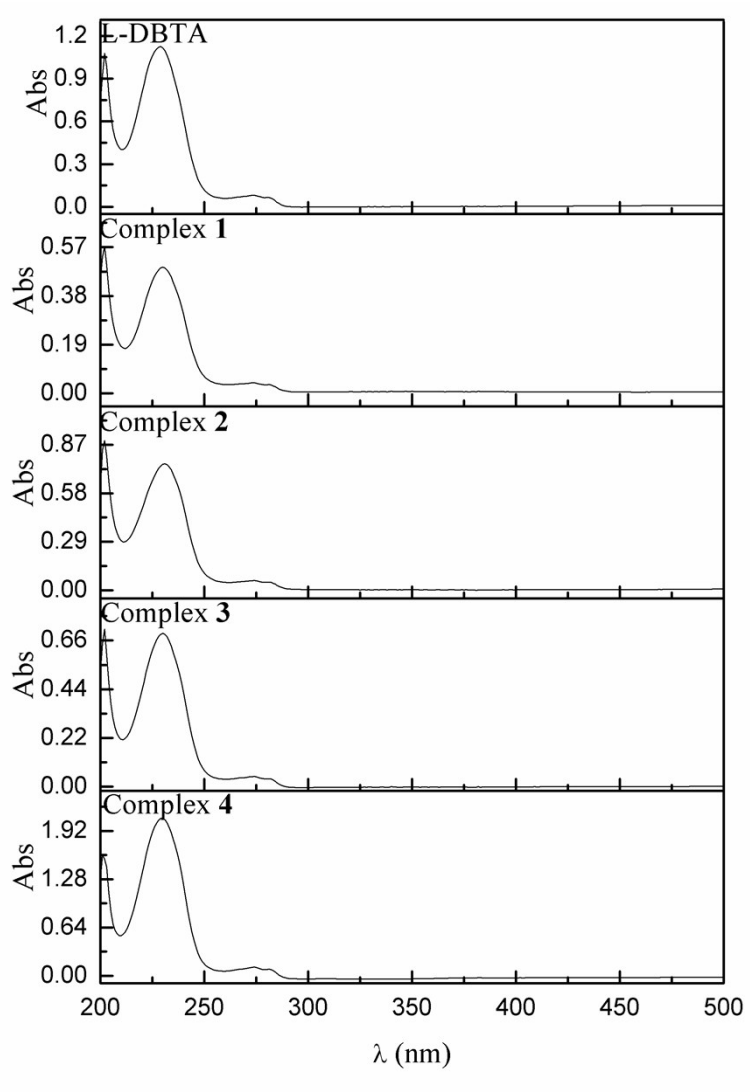

Figure S3. UV-vis spectra of L-DBTA and complexes **1**–**4** in methanol

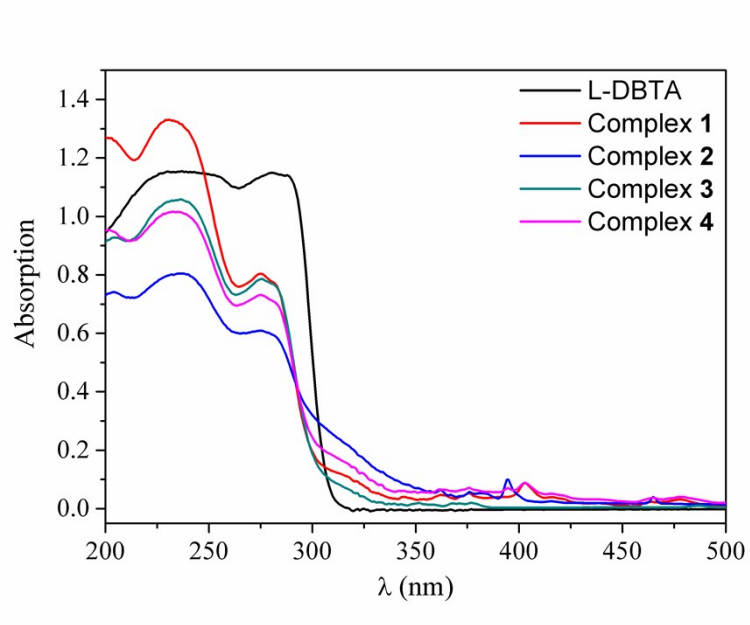

Figure S4. UV diffused reflectance of solid-state L-DBTA and complexes **1** – **4**

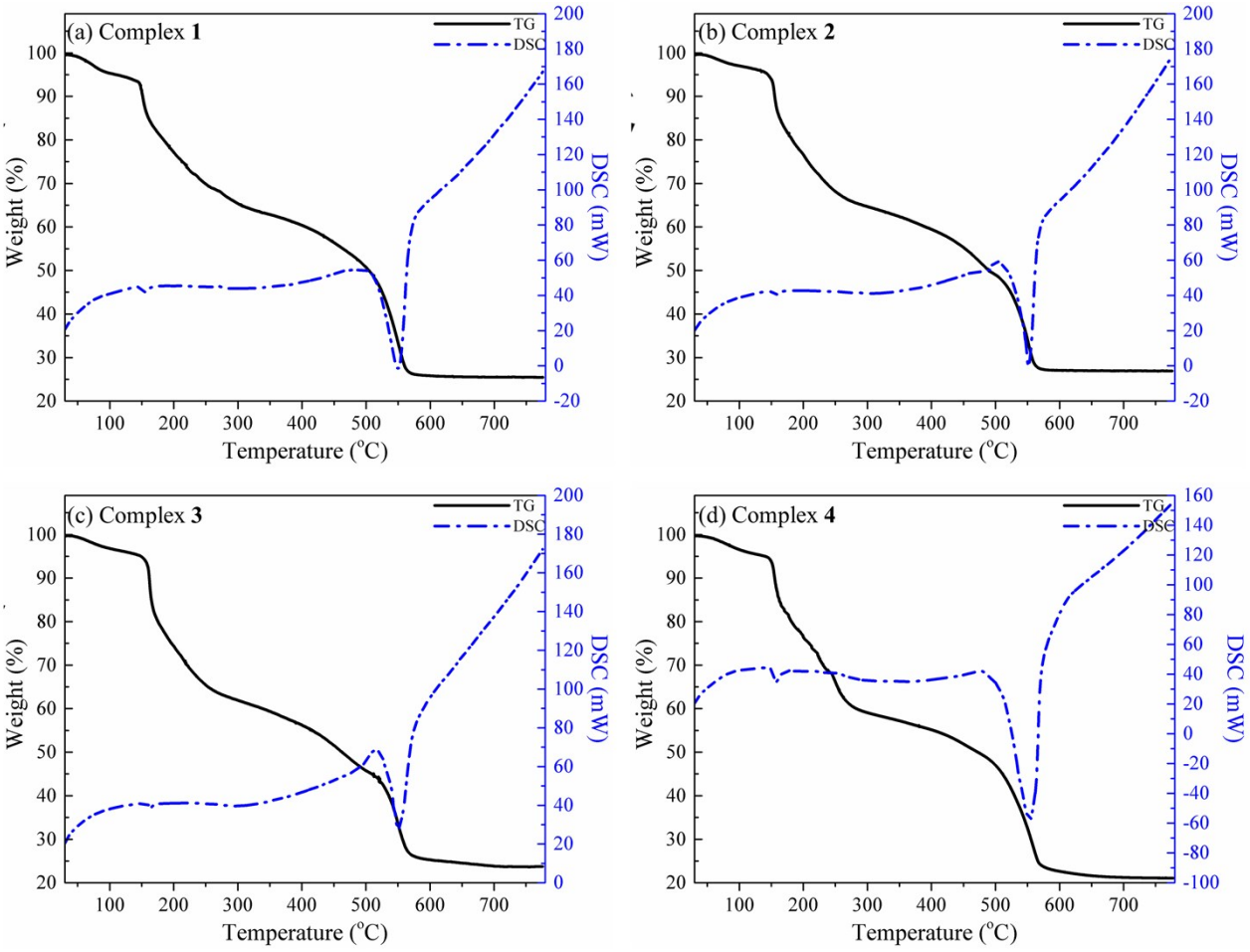

Figure S5. TG-DSC curves of complexes **1** – **4**

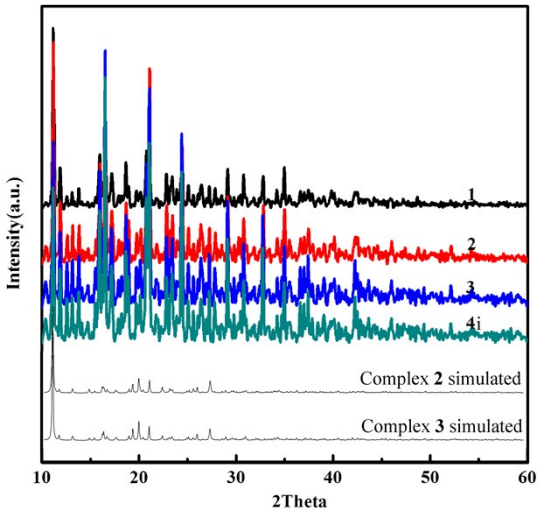

Figure S6. PXRD patterns for complexes **1** – **4**

2.4 Luminescent properties of 1 – 4

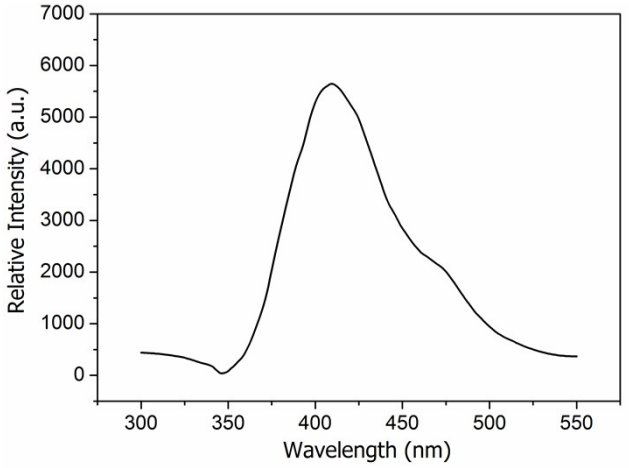

Figure S7. The spectrum of the low temperature phosphorescence of galliu m complex at 77 K

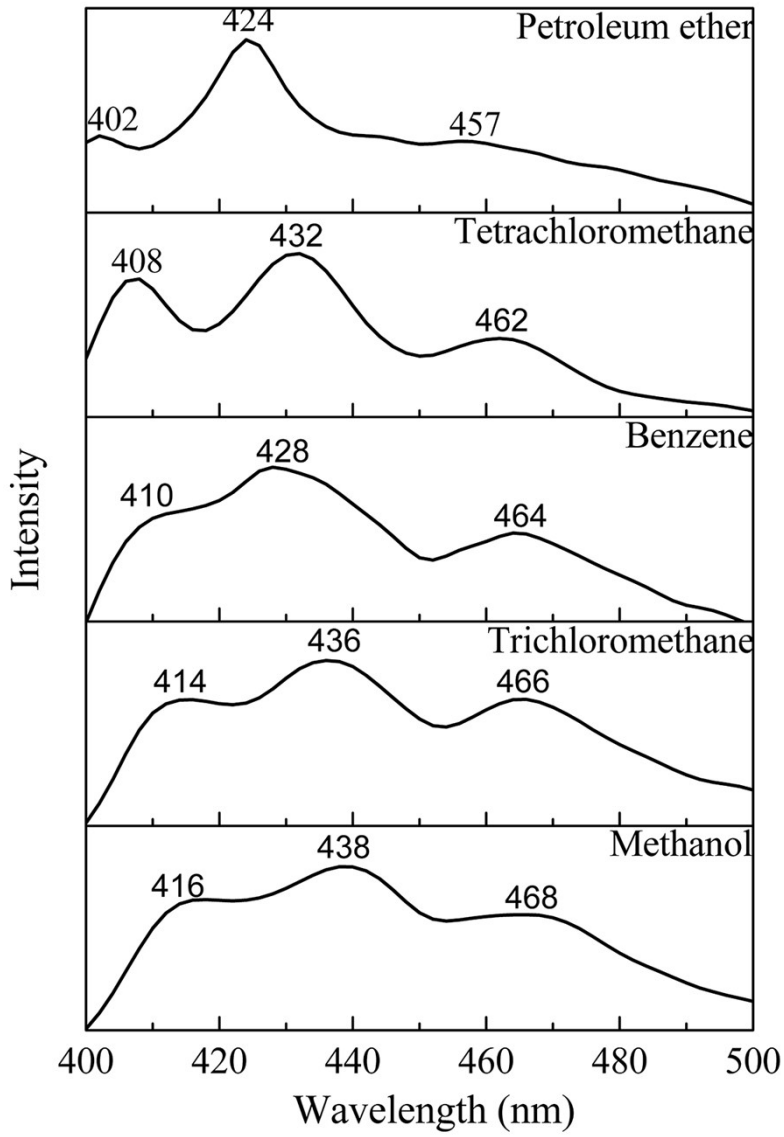

Figure S8. Emission spectra of L-DBTA saturated solution in different polar solvent. Alongwith the polar increase of the solvent, the emission peak apparently red-shift, which suggests that the intramolecular charge-transfer exists in the L-DBTA ligand. Comparing with singlet excited state (S_1^*) tested by UV spectra, IMCT excited state usually possesses lower energy levels and absorbs longer excitation wavelength, which is an explanation to the mismatch of absorption bands between the UV spectra (228 nm) and excitation spectra (438 nm).

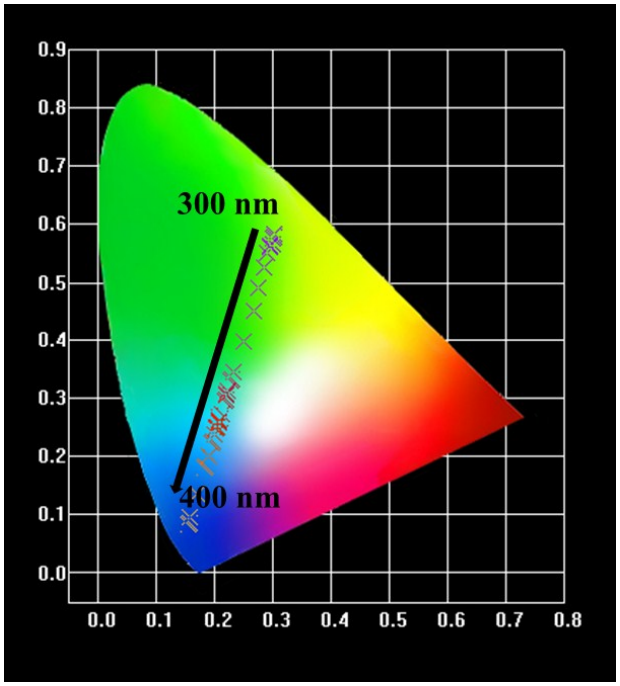

Figure S9. CIE-1931 chromaticity diagram showing the emissions of complex **3** varying from green to cyan and to blue by changing the excitation wavelength

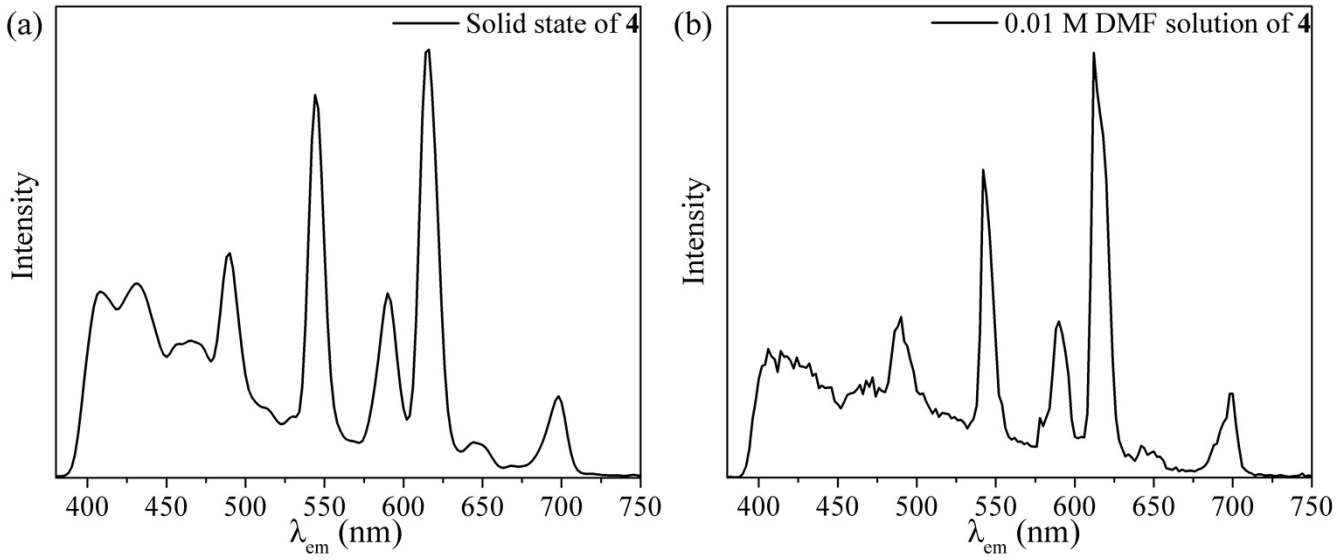

Figure S10. Emission spectrum of (a) solid-state and (b) 0.01 M DMF solution of **4** excited at 322 nm

Table S3. Color, CIE coordination, lifetimes and quantum yields of complex **1** – **4**

No.	λ_{ex} (nm)	Colour	CIE	τ (ms)			Φ (%)
				438 nm	544 nm	614 nm	
1	378	blue	0.157;0.112	1.1E-3[a]	-	-	2.21
2	394	red	0.586;0.321	-	-	0.31	8.20
3	380	green	0.291;0.550	-	1.07	-	29.1
4	322	white	0.333;0.334	8.4E-4[a]	0.65	0.12	6.50
Ag^{+}@**4**	322	red	0.408;0.358	7.8E-4[a]	6.5E-2[a]	4.2E-3[a]	-[b]
Mn^{2+}@**4**	322	blue	0.207;0.194	8.0E-3[a]	5.6E-2[a]	1.0E-2[a]	-[b]

[a] only τ_1 is provided
[b] the data could be obtained

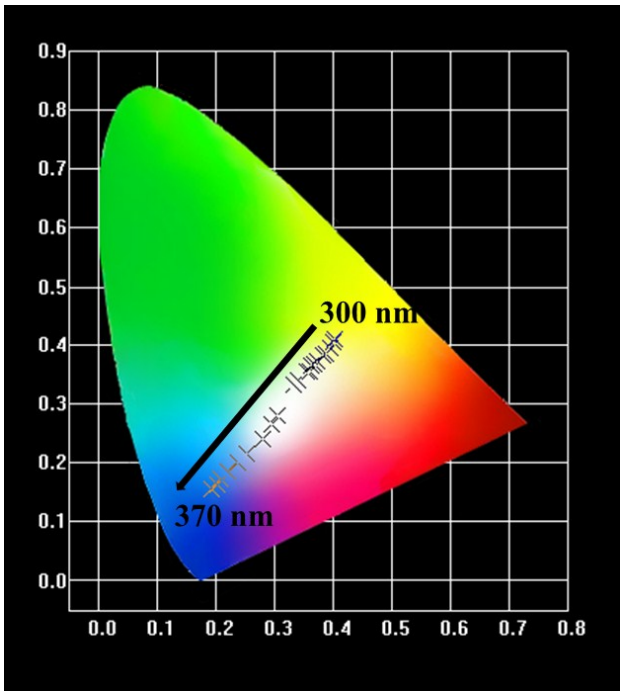

Figure S11. CIE-1931 chromaticity diagram showing the emissions of complex **4** varying from yellow to white and to blue by changing the excitation wavelength

2.5 Ag^{+} and Mn^{2+} ions sensing properties of 4

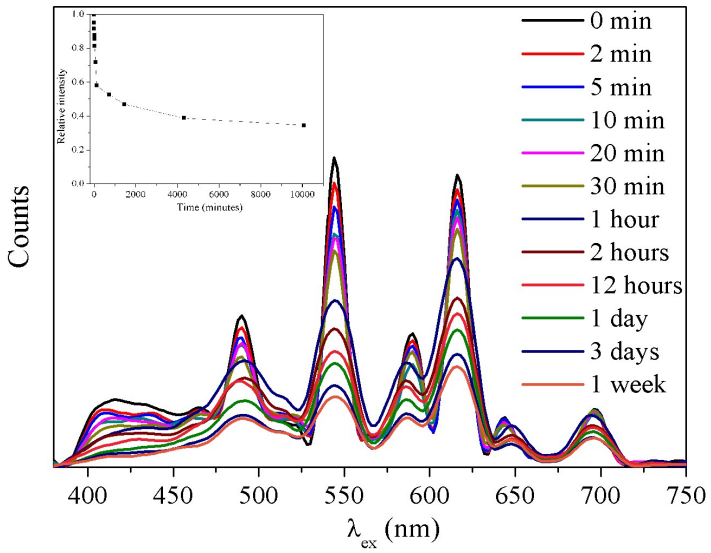

Figure S12. Time-dependence luminescent spectrum of Ag^{+}@**4**. The inset is the relation curve of relative intensity with time

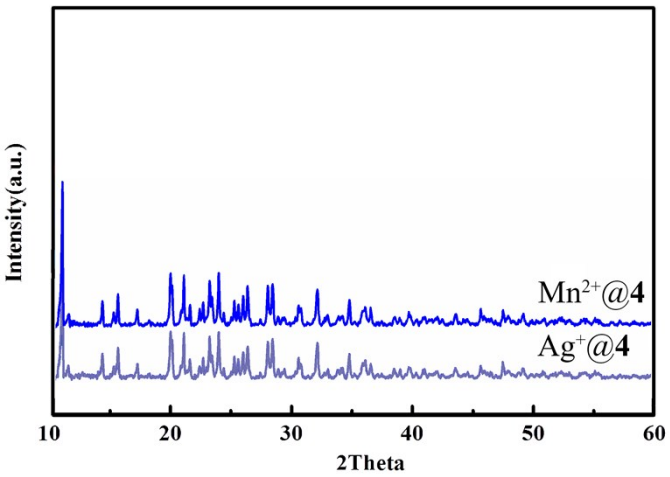

Figure S13. PXRD patterns for Ag^{+}@**4** and Mn^{2+}@**4**

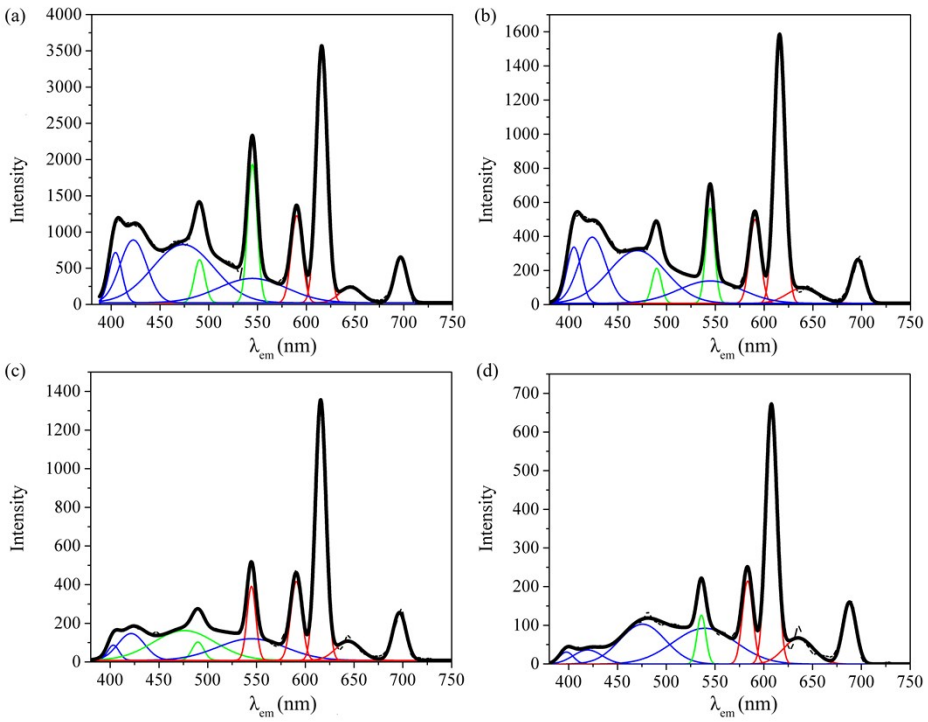

Figure S14. Peak fitting for Ag^{+}@**4** with the Ag^{+} concentration of (a) blank; (b) 5×10^{-8} M; (c) 5×10^{-7} M and (d) 2 M

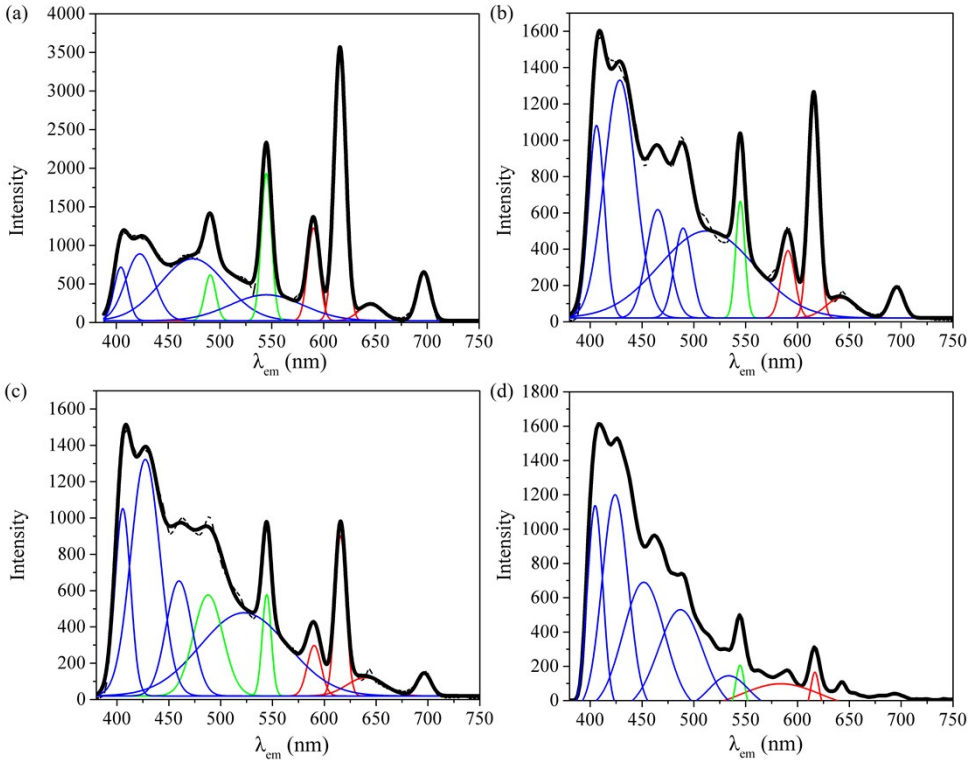

Figure S15 Peak fitting for Mn^{2+}@**4** with the Mn^{2+} concentration of (a) blank; (b) 5×10^{-8} M; (c) 5×10^{-7} M and (d) 2 M.

Table S4. Peak analysis for Ag^+@**4** with distinct Ag^+ concentration

Ag^+ Concentration (M)	wavenumber (nm)	Area	Height	FWHM[a]
Blank	404.4	11483	694	15.5
	422.7	29687	867	32.2
	473.9	63218	804	73.9
	490.7	7980	594	12.6
	544.7	23409	1912	11.5
	544.7	29627	336	82.7
	590.2	16995	1201	13.3
	615.8	48711	3498	13.1
	645.5	5993	212	26.5
	696.7	10100	632	15.0
5×10^{-8}	404.0	5980	330	17.0
	421.8	13434	388	23.5
	473.0	22610	309	68.7
	489.9	2482	205	7.7
	544.7	6340	558	10.7
	544.7	10700	132	76.5
	590.6	6962	492	13.3
	615.7	21071	1537	12.9
	639.6	3625	90	37.9
	696.2	4404	257	16.1
5×10^{-7}	403.3	1152	79	13.8
	421.5	4772	139	32.2
	470.0	12290	154	74.8
	489.9	1438	95.0	14.2
	544.8	4345	383	10.6
	544.8	9765	112	81.8
	590.8	5729	408	13.2
	615.7	17739	1326	12.6
	644.0	3161	98	30.4
	696.6	4216	248	16.0
2	397.7	561	31	16.8
	419.5	1351	37	34.5
	475.5	6051	103	55.0
	536.0	1419	127	10.5
	539.4	7529	93	76.2
	583.4	2874	215	12.6
	607.8	9198	651	13.3
	635.5	2537	67	35.8
	687.8	2715	161	15.9

[a] full width at half maximum

Table S5. Peak analysis for Mn^{2+}@4 with distinct Mn^{2+} concentration

Mn^{2+} Concentration (M)	wavenumber (nm)	Area	Height	FWHM [a]
Blank	404.4	11483	694	15.5
	422.7	29687	867	32.2
	473.9	63218	804	73.9
	490.7	7980	594	12.6
	544.7	23409	1912	11.5
	544.7	29627	336	82.7
	590.2	16995	1201	13.3
	615.8	48711	3498	13.1
	645.5	5993	212	26.5
	696.7	10100	632	15.0
5×10^{-8}	406.1	20144	1060	17.8
	428.6	49345	1310	34.4
	475.1	16272	597	25.6
	492.6	10389	495	19.7
	512.6	55000	480	107.7
	544.7	7147	643	10.4
	590.8	6105	371	15.5
	615.6	15463	1188	12.2
	641.7	3943	110	33.6
	695.7	2896	171	15.9
5×10^{-7}	406.6	19192	1032	17.5
	429.4	45790	1302	33.0
	459.8	19722	633	29.3
	492.9	19798	556	33.4
	522.6	48485	458	99.5
	544.5	6079	559	10.2
	590.2	4622	278	15.6
	615.7	11578	882	12.3
	639.6	4455	101	41.5
	696.4	2098	125.6	15.7
2	408.8	22089	1190	17.4
	434.0	39256	1253	29.4
	461.7	37182	743	47.0
	487.1	31039	583	50.0
	533.7	9491	197.6	45.1
	544.5	2724	259	9.9
	583.9	14329	151	89.0
	616.8	2114	219	9.1
	640.0	802	175	8.7
	696.4	418	66	12.2

[a] full width at half maximum

Reference

[1]. F. Zhang, P. Yan, H. Li, X. Zou, G. Hou and G. Li, *Dalton Trans.*, 2014, **43**, 12574.

[2]. T. Smith and J. Guild, *Trans. Opt. Soc.*, 1931, **33**, 73.

[3]. W. Niu, P. Yan, Z. Fan, N. Fan, J. Sun and G. Li, *Sci. Adv. Mater.*, 2016, **8**, 2189.